Bayesian extraction of HQET parameters from the inclusive semi-leptonic decay of the Λ_c^+ baryon*

Dong Xiao (肖栋)[1] Kangkang Shao (邵康康)[2†]

[1]School of Nuclear Science and Technology, Lanzhou University, Lanzhou 730000, China
[2]School of Physics, Huazhong University of Science and Technology, Wuhan 430074, China

Abstract: We extract the non-perturbative heavy quark effective theory (HQET) parameters from the inclusive semi-leptonic decay $\Lambda_c^+ \to Xe^+\nu_e$. Unlike charmed mesons produced near the threshold, Λ_c^+ baryons produced in e^+e^- annihilation exhibit a complex momentum distribution, which makes the transformation of the electron energy spectrum from the laboratory frame to the Λ_c^+ rest-frame non-trivial. To address this issue, we develop a novel Bayesian inference method to reconstruct the electron energy moments in the Λ_c^+ rest-frame. We determine the HQET parameters $\mu_\pi^2(\Lambda_c^+)$ and $\rho_D^3(\Lambda_c^+)$ for the first time using a purely data-driven approach by performing a global fit of theoretical predictions in the 1S mass scheme to these extracted moments.

Keywords: HQET, non-perturbative parameter, inclusive decay, charmed baryon, Bayesian method

DOI: 10.1088/1674-1137/ae4a09 **CSTR:** 32044.14.ChinesePhysicsC.50063001

I. INTRODUCTION

Recent years have witnessed significant progress in the understanding of heavy-quark dynamics and inclusive decays of heavy hadrons. Accurate theoretical predictions for lifetimes and decay distributions of charm and bottom hadrons play a central role in testing the standard model and in extracting fundamental parameters such as Cabibbo–Kobayashi–Maskawa (CKM) matrix elements [1−4]. In this context, the nonperturbative inputs associated with the heavy-quark expansion (HQE)/heavy quark effective theory (HQET), especially higher-dimensional local-operator matrix elements, are among the dominant sources of theoretical uncertainty.

In the charmed meson sector (such as D^0, D^+, and D_s^+), recent analyses successfully extracted HQET matrix elements by employing the 1S mass scheme to ensure perturbative convergence [5]. Extending this success to the baryon sector is critical. A reliable determination of non-perturbative parameters (e.g., kinetic operator μ_π^2, Darwin operator ρ_{LS}^3, and others) for charmed baryons directly affects our understanding of their lifetime hierarchy [6−8] and the precision of inclusive determinations of CKM elements such as $|V_{cs}|$ and $|V_{cd}|$ [9−13].

However, applying the same strategy as in the meson sector to baryons — specifically to Λ_c^+ — faces a unique experimental challenge. In meson experiments (e.g., at threshold or tagged-meson setups), the Lorentz boost of the parent meson is small or fixed, enabling a straightforward transformation of the measured electron energy spectrum from the lab-frame to the meson rest-frame. In contrast, Λ_c^+ baryons produced in generic e^+e^- annihilation experiments, such as Belle or BESIII, emerge with broad and mixed momentum distributions. Consequently, the observed laboratory-frame electron spectrum is a superposition of many distinct kinematic configurations, which makes the relationship with the Λ_c^+ rest-frame electron energy nontrivial, complicating any attempt to extract rest-frame decay distributions (and thus HQET moments) in a model-independent manner.

In this study, we address this challenge by introducing a novel iterative Bayesian inference framework. We consider the transformation from the laboratory-frame to the Λ_c^+ rest-frame as a probabilistic inverse problem. Instead of relying on fixed-boost approximations or discarding events with large boost uncertainty, our method infers the most probable underlying rest-frame electron energy distribution directly from the full, superimposed laboratory-frame data. Subsequently, we combine this novel extraction method with theoretical calculations that include power corrections up to $O(1/m_c^3)$ and perturbative corrections up to the next-to-next-to-leading-order

Received 9 December 2025; Accepted 25 February 2026; Accepted manuscript online 26 February 2026

* Supported in part by Natural Key R&D Program of China (2023YFA1609400) and National Natural Science Foundation of China (NSFC) (12105127)

† E-mail: kangkshao@gmail.com

(NNLO). This methodology maximizes the extraction of physical information from limited statistics, enabling a precise, model-independent determination of the spectral moments and Λ_c^+ HQET parameters in the presence of complex kinematically mixed data.

The remainder of this paper is organized as follows: Sec. II presents our Bayesian inference approach to obtain the electron energy spectrum in the Λ_c^+ rest-frame and reports the resulting spectrum and electron energy moments. Sec. III discusses the theoretical expressions of the electron energy moments and performs a global fit of these formulas to data to constrain relevant HQET parameters for Λ_c^+. Finally, Sec. IV presents the summary and prospects for the HQET parameters determined from inclusive semi-leptonic decay of charmed hadrons.

II. CALCULATION OF ELECTRON ENERGY MOMENTS IN THE Λ_c^+ REST-FRAME

A. Iterative bayesian inference methodology

The analysis of the electron energy spectrum in the semi-leptonic decay $\Lambda_c^+ \to Xe^+\nu_e$ provides crucial insights into the form factors and internal structure of the Λ_c^+ baryon [14]. The data were collected at seven distinct center-of-mass energies ($\sqrt{s}$) ranging from 4.6 to 4.7 GeV at BESIII, where $e^+e^- \to \Lambda_c^+\bar{\Lambda}_c^-$ occurs. The experimentally measured electron momentum distribution in the laboratory frame is a composite spectrum, aggregating data from all energy points.

A direct transformation of this combined lab-frame spectrum to the Λ_c^+ rest-frame is unfeasible because of several complicating factors, which are listed below.

- **Varying Boosts:** The Λ_c^+ baryons are produced with different Lorentz boosts at each of the seven energy points.

- **Varying Polarization:** The longitudinal polarization (α_0) of Λ_c^+ is energy-dependent, which affects its production angle and the kinematics of the daughter electron in the lab-frame.

- **Detector Effects:** The measured spectrum is distorted by the finite geometric acceptance and reconstruction efficiency of the detector.

To address these challenges, we employ an iterative Bayesian inference technique, illustrated in Fig. 1. This method uses a Monte Carlo (MC) simulation to model the entire process from a hypothesized true electron spectrum in the Λ_c^+ rest-frame to the measured electron spectrum in the lab-frame. Further, it iteratively refines the hypothesis until the simulation matches the data.

The core of the analysis is an iterative procedure based on the principles of Bayes' theorem, as pioneered by D'Agostini [15].

B. Monte Carlo simulation

A detailed MC simulation is the engine of the Bayesian procedure. For each iteration, a large sample of events is generated following these steps listed below.

1. **Energy Point Sampling:** An energy point ($\sqrt{s}$) is randomly selected, weighted by the measured single-tag yields of $\bar{\Lambda}_c^-$ at each point, ensuring the correct mixture of production conditions.

2. Λ_c^+ **Generation (lab-frame):** A four-momentum for the parent Λ_c^+ is generated in the laboratory frame. This step correctly models the production angular distribution, which is proportional to $1+\alpha_0(\sqrt{s})\cos^2\theta$, using the experimentally measured energy-dependent polarization parameter $\alpha_0(\sqrt{s})$. A small transverse boost of the e^+e^- system is also included.

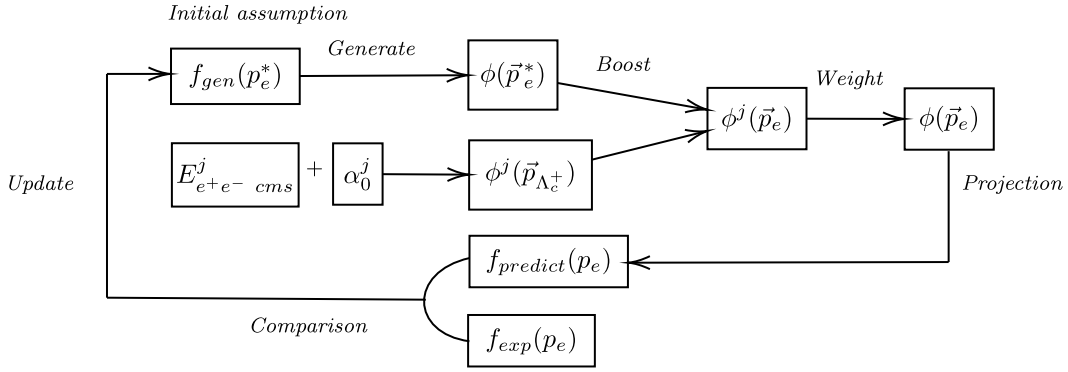

Fig. 1. Flowchart illustrating the iterative Bayesian inference method. The process starts with an arbitrary assumption for the electron momentum probability density function (PDF) in the Λ_c^+ rest-frame, which is refined by comparing the resulting simulated laboratory-frame PDF with experimental data. Here, f represents the one-dimensional normalized PDF of electron momentum, while ϕ represents the PDF in the three momentum vector space. p and $\vec{p}$ represent the variables in the laboratory frame, whereas p^* and $\vec{p}^{\,*}$ represent the variables in the Λ_c^+ rest-frame.

3. **Electron Generation (Λ_c^+ rest-frame):** An electron momentum p_e^* is randomly sampled from the current hypothesis for the "origin" spectrum, $f_{\rm gen}(p_e^*)$. A four-momentum is then constructed assuming isotropic decay in the Λ_c^+ rest-frame, which is distributed as $\phi(\vec{p}_e^*)$.

4. **Transformation to lab-frame:** The four-momentum of the electron is then Lorentz-boosted from the Λ_c^+ rest-frame to the laboratory frame.

5. **Detector Emulation:** A cut on the lab-frame polar angle of the electron, $|\cos\theta_{\rm lab}| < 0.93$, is applied to emulate the geometric acceptance of the detector.

This process produces a predicted lab-frame spectrum, $f_{\rm predict}(p_e)$, and a migration matrix $\mathcal{M}$, which maps the relationship between the generated electron momentum in the Λ_c^+ rest-frame and the observed electron momentum in lab-frame.

C. Iterative procedure

The iteration procedure is performed as follows. For each iteration k:

1. Generate a MC sample based on the current hypothesis of electron momentum distribution in the Λ_c^+ rest-frame, $f_{\rm gen}^k(p_e^*)$, to produce a predicted lab-frame spectrum, $f_{\rm predict}^k(p_e)$, and a migration matrix $\mathcal{M}^k$. The element $\mathcal{M}_{ij}^k$ is defined as the number of electrons observed in the j-th momentum bin in the lab-frame that originated from the i-th momentum bin in the Λ_c^+ rest-frame. Physically, the migration matrix is the discretized detector-and-kinematics response that encodes the conditional probability $P\left(p_e \in j \,\middle|\, p_e^* \in i\right)$. Its dominant origin is the Lorentz boost from the Λ_c^+ rest-frame to the laboratory frame, as well as the effects of the $\sqrt{s}$-dependent Λ_c^+ polarization and detector acceptance effects.

2. Calculate the efficiency, ε_i^k, of observing an electron generated within the i-th momentum bin of the Λ_c^+ rest-frame.

$$\varepsilon_i^k = \frac{\sum_j \mathcal{M}_{ji}^k}{N_{{\rm gen},i}^k}. \tag{1}$$

3. Estimate the Bayesian probability, $P^k(i|j)$, that an electron observed in j-th lab-frame momentum bin originated from the i-th momentum bin in the Λ_c^+ rest-frame.

$$P^k(i|j) = \frac{\mathcal{M}_{ij}^k}{\sum_i \mathcal{M}_{ij}^k}. \tag{2}$$

4. Update the hypothesis for the electron momentum distribution in the Λ_c^+ rest-frame for the next iteration based on the experimentally measured distribution in the lab-frame.

$$f_{{\rm gen},i}^{k+1}(p_e^*) = \frac{1}{\varepsilon_i^k} \cdot \sum_j f_{{\rm exp},j}(p_e) \cdot P^k(i|j), \tag{3}$$

where $f_{{\rm exp},j}(p_e)$ represents the content of the j-th bin of the experimental data.

For each iteration, we generate 10,000,000 events containing the information of the four-momentum vector of the electron in the Λ_c^+ rest-frame and the four-momentum vector of Λ_c^+ in the lab-frame weighted at seven distinctive CMS energies. Then, we repeat steps from 1 to 4 until the $\chi^2/n_{\rm d.o.f.}$ between the predicted $f_{\rm predict}(p_e)$ and measured $f_{\rm exp}(p_e)$ converges to 1.

D. Low-momentum theoretical constraint

The experimental data contain no information below $p_e = 0.2$ GeV. We constrain the unfolded spectrum for $p_e^* < 0.2$ GeV with a smooth theoretical form motivated by the well-behaved HQE away from the endpoint, $f\left(p_e^*\right) \propto \left(p_e^*\right)^2 \left(1 + b p_e^*\right) \left(1 - p_e^*\right)$, The parameter b is fitted to the first four bins above 0.2 GeV in each Bayesian iteration, and first-derivative (C^1) matching is imposed at $p_e^* = 0.2$ GeV, ensuring a smooth transition between the theory-driven and data-driven regions of the spectrum.

E. Electron momentum distribution

The iterative procedure converges after 4 iterations, at which point the $\chi^2/n_{\rm d.o.f.}$ between the final simulated spectrum and experimental data stabilizes at 0.74. The final comparison is shown in Fig. 2(a). The Bayesian inferred electron momentum spectrum in the Λ_c^+ rest-frame is shown in Fig. 2(b).

F. Nominal results of electron energy moments

The first four terms of the electron energy moments of the decay of $\Lambda_c^+ \to X e^+ \nu_e$ are defined by integration over the energy spectrum E_e^* in the Λ_c^+ rest-frame.

$$\begin{aligned}
\langle E_e \rangle &= \frac{1}{\Gamma_{\Lambda_c^+}} \int \frac{{\rm d}\Gamma}{{\rm d}E_e^*} E_e^* {\rm d}E_e^* \\
\langle E_e^2 \rangle_{\rm center} &= \frac{1}{\Gamma_{\Lambda_c^+}} \int \frac{{\rm d}\Gamma}{{\rm d}E_e^*} (E_e^* - \langle E \rangle)^2 {\rm d}E_e^* \\
\langle E_e^3 \rangle_{\rm center} &= \frac{1}{\Gamma_{\Lambda_c^+}} \int \frac{{\rm d}\Gamma}{{\rm d}E_e^*} (E_e^* - \langle E \rangle)^3 {\rm d}E_e^* \\
\langle E_e^4 \rangle_{\rm center} &= \frac{1}{\Gamma_{\Lambda_c^+}} \int \frac{{\rm d}\Gamma}{{\rm d}E_e^*} (E_e^* - \langle E \rangle)^4 {\rm d}E_e^*
\end{aligned} \tag{4}$$

Upon integration, we obtain the following values for the electron energy moments: $\langle E_e \rangle = 0.455$ GeV, $\langle E_e^2 \rangle_{\rm center} = 2.75 \times 10^{-2}$ GeV^2, $\langle E_e^3 \rangle_{\rm center} = -3.67 \times 10^{-4}$ GeV^3, and $\langle E_e^4 \rangle_{\rm center} = 1.89 \times 10^{-3}$ GeV^4.

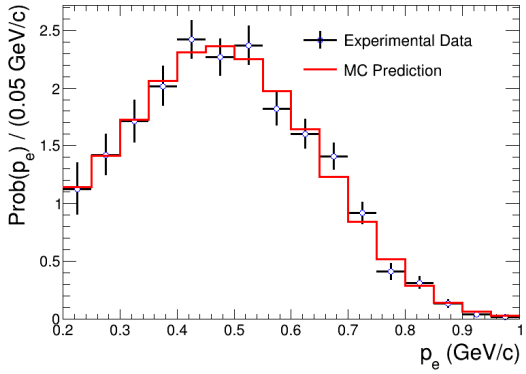

(a) Comparison between simulated and measured PDF of p_e in lab-frame, with $\chi^2/n_{\rm d.o.f.} = 0.74$.

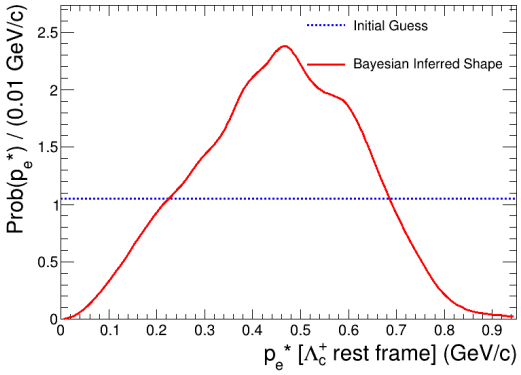

(b) Bayesian inferred PDF of p_e^* in Λ_c^+ rest-frame, with the initial assumption of a flat distribution.

Fig. 2. (color online) Result of the electron momentum distribution of $\Lambda_c^+ \to Xe^+\nu_e$.

G. Statistical uncertainty

The statistical uncertainty on the inferred electron energy moments attributed to the finite statistics of the input data is determined using a "bootstrap" method. The resulting statistical covariance matrix is listed in Table 1

1. A large number ($N_{\rm toys} = 10000$) of "toy" experimental spectra are generated by fluctuating the content of each bin of the original data according to a Gaussian distribution defined by its central value and error.

2. The entire iteration procedure is performed for each toy spectrum.

3. The statistical error on each final moment is taken as the root mean square (RMS) of the distribution of that moment over all toy experiments.

4. The full 4×4 statistical covariance matrix between the moments is also computed from this ensemble.

H. Systematic uncertainties

The dominant systematic uncertainties in this Bayesian inference procedure are attributed to three primary sources: the choice of the number of iterations, initial shape assumed for the distribution in Λ_c^+ rest-frame, and experimental uncertainties on the polarization parameters (α_0). We employ a grid scan approach to robustly estimate these uncertainties and account for potential correlations between them. The corresponding systematic covariance matrix is listed in Table 2.

We define a set of discrete variations for each of the three main sources:

1. **Number of Iterations:** The number of Bayesian iterations is varied across three choices: {3, 4, 5}, centered around our nominal choice of 4.

2. **Initial Shape:** Three distinct functional forms are used for the initial guess of the true spectrum: a flat distribution (nominal), polynomial function, and sine function.

3. **Polarization Parameter (α_0):** The set of $\alpha_0(\sqrt{s})$ parameters is varied according to its total experimental uncertainty: {Nominal - 1σ, Nominal, Nominal + 1σ}.

The full procedure is performed for all $3\times3\times3 = 27$ combinations of these discrete choices. This ensemble of 27 output moment sets, $\{\langle E_e\rangle, \langle E_e^2\rangle_{\rm center}, \langle E_e^3\rangle_{\rm center}, \langle E_e^4\rangle_{\rm center}\}$, represents the space of systematic model variations.

The total systematic uncertainty for each moment is defined as the RMS of this distribution. Furthermore, this method allows for the calculation of the full 4×4 systematic covariance matrix, capturing the correlations in how the moments shift together as the analysis assumptions are varied.

Table 1. Statistical covariance matrix for the four electron energy moments determined by the bootstrap method.

Stat. Cov.	$\langle E_e\rangle$/ GeV	$\langle E_e^2\rangle_{\rm center}$/ GeV^2	$\langle E_e^3\rangle_{\rm center}$/ GeV^3	$\langle E_e^4\rangle_{\rm center}$/ GeV^4
$\langle E_e\rangle$/ GeV	2.472×10^{-4}	-5.315×10^{-5}	4.762×10^{-6}	-6.735×10^{-6}
$\langle E_e^2\rangle_{\rm center}$/ GeV^2	-5.315×10^{-5}	1.314×10^{-5}	-1.206×10^{-6}	1.634×10^{-6}
$\langle E_e^3\rangle_{\rm center}$/ GeV^3	4.762×10^{-6}	-1.206×10^{-6}	1.926×10^{-7}	-1.404×10^{-7}
$\langle E_e^4\rangle_{\rm center}$/ GeV^4	-6.735×10^{-6}	1.634×10^{-6}	-1.404×10^{-7}	2.011×10^{-7}

Table 2. Systematic covariance matrix for the four electron energy moments determined by the grid scan method.

Sys. Cov.	$\langle E_e\rangle$/ GeV	$\langle E_e^2\rangle_{\rm center}$/ GeV^2	$\langle E_e^3\rangle_{\rm center}$/ GeV^3	$\langle E_e^4\rangle_{\rm center}$/ GeV^4
$\langle E_e\rangle$/ GeV	7.031×10^{-6}	-1.716×10^{-6}	1.914×10^{-7}	-1.791×10^{-7}
$\langle E_e^2\rangle_{\rm center}$/ GeV^2	-1.716×10^{-6}	4.462×10^{-7}	-3.776×10^{-8}	4.722×10^{-8}
$\langle E_e^3\rangle_{\rm center}$/ GeV^3	1.914×10^{-7}	-3.776×10^{-8}	8.364×10^{-9}	-1.412×10^{-9}
$\langle E_e^4\rangle_{\rm center}$/ GeV^4	-1.791×10^{-7}	4.722×10^{-8}	-1.412×10^{-9}	6.578×10^{-9}

I. Final results of the electron energy moments

After considering the statistical and systematic uncertainties, we obtain the final result of the electron energy moments of $\Lambda_c^+\to Xe^+\nu_e$ based on the Bayesian inference approach. The Bayesian inferred electron momentum distribution in the Λ_c^+ rest-frame with an error band is shown in Fig. 3(a). The migration matrix is shown in Fig. 3(b). The sizable off-diagonal population at larger momenta indicates that a fixed p_e^* bin can migrate into a broad range of $p_e^{\rm lab}$ values, reflecting the stronger effects of boost in the high-momentum region. This behavior implies that a naive identification of the laboratory-frame spectrum with the rest-frame spectrum is not reliable: the observed distribution is a non-trivial convolution of the underlying rest-frame spectrum with the kinematic response. Our iterative Bayesian procedure treats the problem as an inverse one and uses the migration information to probabilistically reconstruct the rest-frame spectrum from the laboratory frame data, which is essential for any quantitative rest-frame interpretation based on the extracted spectrum.

The integrated results of the first four electron energy moments of $\Lambda_c^+\to Xe^+\nu_e$ with statistical and systematic uncertainties are listed in Table 3.

Table 3. The first four electron energy moments of $\Lambda_c^+\to Xe^+\nu_e$. The first uncertainty is statistical, and the second is systematic.

Energy Moment	Value
$\langle E_e\rangle$/GeV	$(4.55\pm0.16\pm0.03)\times10^{-1}$
$\langle E_e^2\rangle_{\rm center}$/GeV^2	$(2.75\pm0.37\pm0.07)\times10^{-2}$
$\langle E_e^3\rangle_{\rm center}$/GeV^3	$(-3.67\pm4.39\pm0.91)\times10^{-4}$
$\langle E_e^4\rangle_{\rm center}$/GeV^4	$(1.89\pm0.45\pm0.08)\times10^{-3}$

III. PHENOMENOLOGICAL ANALYSIS OF INCLUSIVE Λ_c^+ DECAYS

A. Theoretical formulas

Similar to the meson case, the inclusive decay of Λ_c^+ is described within the framework of HQE, where the short-distance coefficients are computed perturbatively, and the resulting expressions are organized as a double expansion in $\Lambda_{\rm QCD}/m_c$ and α_s with the strange-quark mass treated as a quantity of order $\Lambda_{\rm QCD}$. For our theoretical formulas, the power corrections are included up to order $(\Lambda_{\rm QCD}/m_c)^3$. For the leading-power contributions, we incorporate α_s corrections up to NNLO, whereas for the higher-power terms, only the leading-order contributions are considered. In comparison to the D-meson case, the HQE for Λ_c^+ involves a different pattern of non-perturbative matrix elements: the chromomagnetic and spin-orbit contributions, μ_G^2 and ρ_{LS}^3, vanish in Λ_c^+ because of the spin-zero configuration of the light diquark [16]. Con-

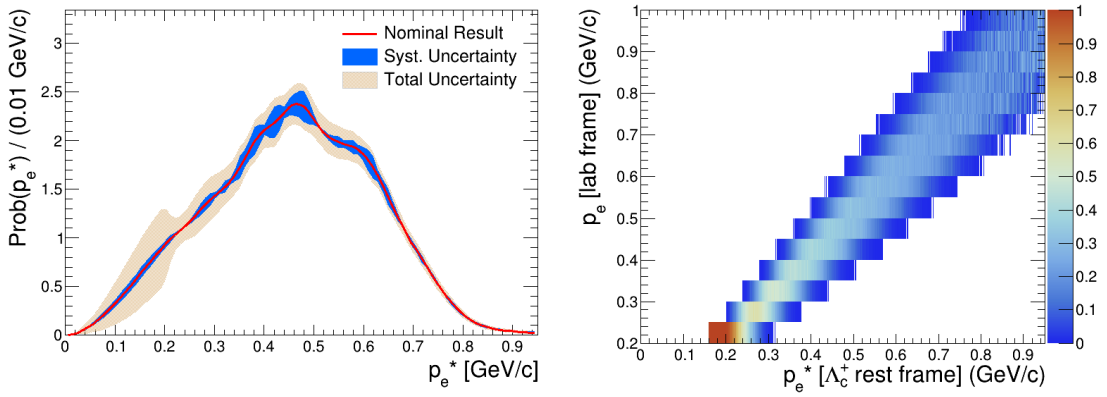

(a) Final unfolded result of the electron momentum distribution of $\Lambda_c^+\to Xe^+\nu_e$ in the Λ_c^+ rest-frame. (b) Migration matrix between electron momentum in the Λ_c^+ rest-frame and laboratory frame.

Fig. 3. (color online) Final unfolded result and migration matrix.

sequently, the Darwin term, together with several four-quark operators, play a more prominent role. We adopt the 1S mass scheme in our analysis because it provides notably better convergence in the perturbative expansion for charm inclusive decays [5].

Within the pole mass scheme, the decay widths can be expressed as

$$\Gamma_{\Lambda_c^+} = \sum_{q=d,s} \hat{\Gamma}_0 \left|V_{cq}\right|^2 m_c^5 \left\{1 + \frac{\alpha_s}{\pi}\frac{2}{3}\left(\frac{25}{4} - \pi^2\right) + \frac{\alpha_s^2}{\pi^2}\left[\frac{\beta_0}{4}\frac{2}{3}\left(\frac{25}{4} - \pi^2\right)\log\left(\frac{\mu^2}{m_c^2}\right) + 2.14690 n_l - 29.88311\right]\right.$$
$$\left. - 8\rho\delta_{sq} - \frac{1}{2}\frac{\mu_\pi^2(\Lambda_c^+)}{m_c^2} + \left(\frac{20}{3} + 8\log\left(\frac{\mu^2}{m_c^2}\right)\right)\frac{\rho_D^3\left(\Lambda_c^+\right)}{m_c^3} + \frac{\tau_0(\Lambda_c^+)}{m_c^3} + \ldots\right\}, \tag{5}$$

where $\hat{\Gamma}_0 = G_F^2/(192\pi^3), V_{cq}$ represents the CKM matrix element, and $\rho = m_s^2/m_c^2$. The quantities $\tau_{\Lambda_c^+} = 128\pi^2 \times \left(T_1\left(\Lambda_c^+\right) - T_2\left(\Lambda_c^+\right)\right)$ denote contributions from the four-quark matrix elements for Λ_c^+ [17]. The QCD coefficient is $\beta_0 = 11 - 2n_f/3$, and we use $n_f = 4$. For the definitions of the local operator matrix elements, we follow the convention of Ref. [17].

For the initial four raw moments, the theoretical expressions are

$$\langle E_e\rangle = \frac{\hat{\Gamma}_0}{\Gamma_{\Lambda_c^+}} \sum_{q=d,s} \left|V_{cq}\right|^2 m_c^6 \left[\frac{3}{10} + \frac{\alpha_s}{\pi}a_1^{(1)} + \frac{\alpha_s^2}{\pi^2}a_1^{(2)} - 3\rho\delta_{sq} + \left(\frac{77}{15} + 4\log\left(\frac{\mu^2}{m_c^2}\right)\right)\frac{\rho_D^3\left(\Lambda_c^+\right)}{m_c^3} + \frac{\tau_0(\Lambda_c^+)}{2m_c^3} + \ldots\right],$$
$$\langle E_e^2\rangle = \frac{\hat{\Gamma}_0}{\Gamma_{\Lambda_c^+}} \sum_{q=d,s} \left|V_{cq}\right|^2 m_c^7 \left[\frac{1}{10} + \frac{\alpha_s}{\pi}a_2^{(1)} + \frac{\alpha_s^2}{\pi^2}a_2^{(2)} - \frac{6}{5}\rho\delta_{sq} + \frac{1}{12}\frac{\mu_\pi^2(\Lambda_c^+)}{m_c^2} + \left(\frac{181}{60} + 2\log\left(\frac{\mu^2}{m_c^2}\right)\right)\frac{\rho_D^3\left(\Lambda_c^+\right)}{m_c^3} + \frac{\tau_0(\Lambda_c^+)}{4m_c^3} + \ldots\right],$$
$$\langle E_e^3\rangle = \frac{\hat{\Gamma}_0}{\Gamma_{\Lambda_c^+}} \sum_{q=d,s} \left|V_{cq}\right|^2 m_c^8 \left[\frac{1}{28} + \frac{\alpha_s}{\pi}a_3^{(1)} + \frac{\alpha_s^2}{\pi^2}a_3^{(2)} - \frac{1}{2}\rho\delta_{sq} + \frac{1}{14}\frac{\mu_\pi^2\left(\Lambda_c^+\right)}{m_c^2} + \left(\frac{233}{140} + \log\left(\frac{\mu^2}{m_c^2}\right)\right)\frac{\rho_D^3\left(\Lambda_c^+\right)}{m_c^3} + \frac{\tau_0(\Lambda_c^+)}{8m_c^3} + \ldots\right],$$
$$\langle E_e^4\rangle = \frac{\hat{\Gamma}_0}{\Gamma_{\Lambda_c^+}} \sum_{q=d,s} \left|V_{cq}\right|^2 m_c^9 \left[\frac{3}{224} + \frac{\alpha_s}{\pi}a_4^{(1)} + \frac{\alpha_s^2}{\pi^2}a_4^{(2)} - \frac{3}{14}\rho\delta_{sq} + \frac{3}{64}\frac{\mu_\pi^2\left(\Lambda_c^+\right)}{m_c^2} + \left(\frac{1989}{2240} + \frac{1}{2}\log\left(\frac{\mu^2}{m_c^2}\right)\right)\frac{\rho_D^3\left(\Lambda_c^+\right)}{m_c^3} + \frac{\tau_0(\Lambda_c^+)}{16m_c^3} + \ldots\right], \tag{6}$$

where the coefficients follow the conventions of Ref. [5]. They are highly sensitive to the charm quark mass m_c. Although HQET is often formulated in the pole-mass scheme, this choice is not suitable for precision analyses because the decay width suffers from a renormalon ambiguity. In the $\overline{\rm MS}$ scheme, the perturbative expansion converges rather slowly [18–21]. For the kinetic mass scheme, contributions scaling as $(\alpha_s/\pi)\mu^n/m_c^n$ arise from the nth-order power corrections in the HQE, and the choice of the cutoff scale μ introduces an additional subtlety [17, 22].

In contrast, the 1S mass scheme avoids the renormalon ambiguity of the pole mass and shows a considerably better perturbative behavior than that of the $\overline{\rm MS}$ and kinetic schemes. Its perturbative series is known to be more stable, and the residual scale dependence is substantially reduced [23–25]. Therefore, the 1S mass scheme provides the most reliable input for the inclusive Λ_c^+ analysis and is adopted throughout this work.

The pole mass m_c is related to the 1S mass $m_{c,1S}$ through [5]

$$m_c = m_{c,1S} + m_{c,1S}\frac{\alpha_s(\mu)^2 C_F^2}{8} \times \left\{1 + \frac{\alpha_s}{\pi}\left[\left(-\log\left(\alpha_s(\mu) m_{c,1S} C_F/\mu\right) + \frac{11}{6}\right)\beta_0 - 4 + \frac{\pi}{8}C_F\alpha_s\right] + \ldots\right\}. \tag{7}$$

We replace the pole mass in Eqs. (5) and (6) with the 1S-mass relation in Eq. (7), and then, we expand the results up to $O(\alpha_s^2)$. In fact, it is worth noting that the next-leading order (NLO) correction constitutes the leading order contribution because the ε-expansion starts at NLO [23].

In addition, to suppress the correlations among the experimental data points, we use the electron-energy central moments rather than the raw moments. The experi-

Table 4. χ^2 fitting results in the $1S$ mass scheme. The χ^2/d.o.f. in the fit, along with the central values and uncertainties for the HQET parameters, are displayed. The first uncertainty arises from experiment data, the second from the evolution of renormalization scale μ from 1 to 2.54 GeV, and the last is attributed to unknown higher order power corrections.

$\mu_\pi^2/(10^{-1}\ \mathrm{GeV}^2)$	$\rho_D^3/(10^{-4}\ \mathrm{GeV}^3)$	$\tau_{\mathrm{WA}}/10^{-1}\ \mathrm{GeV}^3$	χ^2/d.o.f.	N_{data} v.s. N_{param}
$1.33 \pm 0.18 \pm 0.02 \pm 0.40$	$-2.95 \pm 2.59 \pm 0.36 \pm 1.18$	$-2.69 \pm 0.33 \pm 0.12 \pm 0.81$	0.53	5 v.s. 3

mental data inputs

$$\left\{\Gamma_{\Lambda_c^+},\ \langle E_e\rangle,\ \langle E_e^2\rangle_{\mathrm{center}},\ \langle E_e^3\rangle_{\mathrm{center}},\ \langle E_e^4\rangle_{\mathrm{center}}/\langle E_e^2\rangle_{\mathrm{center}}^2\right\}$$

are then employed in the global fit.

B. Toward an extraction of the kinetic energy and Darwin terms

To obtain experimental data points required to constrain the basic HQET parameters of Λ_c^+, we develop and employ a Bayesian inference method to reconstruct the electron-energy moments in the Λ_c^+ rest-frame, providing precise experimental inputs for the fit. These reconstructed moments serve as the experimental inputs for our global analysis. The corresponding theoretical expressions used in this fit are given in Eqs. (5) and (6).

Numerical inputs required for our analysis are derived from well-established lattice and perturbative QCD determinations. For the strange-quark mass, we employ the 2+1+1 FLAG average $\overline{m}_s(2\ \mathrm{GeV}) = (93.44 \pm 0.68)$ MeV, as reported in Ref. [26]. The strong coupling at the charm scale is fixed to $\alpha_s(\overline{m}_c) = 0.387$, following the determination of Ref. [27] based on the `RunDec` evolution package [28]. The scale-dependent quantities $\alpha_s(\mu)$ and $\overline{m}_c(\mu)$ are evaluated for renormalization scales in the interval $1\ \mathrm{GeV} \le \mu \le 2\overline{m}_c(\overline{m}_c)$. For the remaining standard model parameters entering the decay-width and moment calculations, we adopt the PDG 2024 values [29]: $G_F = 1.1663788 \times 10^{-5}$, $|V_{cs}| = 0.975 \pm 0.006$, and $|V_{cd}| = 0.221 \pm 0.004$.

Our χ^2 function is defined as

$$\chi^2(\boldsymbol{\theta}) = (\boldsymbol{y} - \boldsymbol{\eta}(\boldsymbol{\theta}))^{\mathrm{T}} \boldsymbol{V}^{-1} (\boldsymbol{y} - \boldsymbol{\eta}(\boldsymbol{\theta})), \tag{8}$$

where $\boldsymbol{\theta} = \{\mu_\pi^2(\Lambda_c^+), \rho_D^3(\Lambda_c^+), \tau_{\mathrm{WA}}(\Lambda_c^+)\}$ and $\tau_{\mathrm{WA}}(\Lambda_c^+)\} = |V_{cs}|^2 \tau_{0,\mathrm{non-valance}} + |V_{cd}|^2 \tau_{0,\mathrm{valance}}$.

The results[1)] of the global fit are presented in Table 4.

Based on the model-independent method, the fit results obtained in the $1S$ mass scheme are summarized in Table 4. As the current analysis is limited by the number of available experimental and theoretical inputs, we do not attempt a dedicated evaluation of uncertainties from unknown higher-order power corrections. Instead, to account for the possible impact of omitted higher-order power corrections, we assign a 30% systematic uncertainty to the fitted results. The fitted values of $\mu_\pi^2(\Lambda_c^+)$ and $\rho_D^3(\Lambda_c^+)$ are consistent with those extracted in the D-meson decay within 1σ under the $1S$ mass scheme [5]. The results presented in Table 4 differ from those obtained using the improved bag-model [7] and the wave-function approach [9]. This discrepancy warrants further investigation in future work.

IV. CONCLUSION

In this study, we introduced a novel Bayesian inference method to reconstruct the electron energy moments in the Λ_c^+ rest-frame. This methodology represents an advancement in handling inclusive semi-leptonic decays where the momentum of the parent particle is not fixed. Beyond the specific case of Λ_c^+, this strategy provides motivation for analyzing other inclusive decays at B-factories and future colliders. By inferring the rest-frame spectrum from a single, kinematically complex laboratory distribution, we demonstrate a robust alternative to traditional tagging or approximate boost techniques.

Combining these reconstructed moments with a global fit of theoretical predictions in the $1S$ mass scheme, we have, for the first time, determined the non-perturbative heavy-quark parameters $\mu_\pi^2(\Lambda_c^+)$ and $\rho_D^3(\Lambda_c^+)$ directly from data. Our analysis demonstrates that a data-driven approach that avoids model dependence is viable and yields stable values for the HQET parameters. These results lay a new foundation for inclusive analyses of charm-baryon decays, bridging semi-leptonic observables with HQET parameter extraction.

ACKNOWLEDGMENTS

We wish to thank Matteo Fael and Wen-Jie Song for enlightening discussions on calculations of electronic energy spectrum, and especially to Fu-Sheng Yu and Yan-Bing Wei for their inspiring discussions on various experimental and theoretical aspects. Special thanks go to Long Chen and Yan-Qing Ma for providing the numerical NNLO corrections to the partonic decay widths and the corresponding electron energy moments.

1) Within the pseudo-data based robustness tests we performed, we found no evidence for over-fitting.

References

[1] D. Friday, E. Gersabeck, A. Lenz *et al*., (2025), arXiv: 2506.15584
[2] M. Egner, M. Fael, A. Lenz *et al*., JHEP **04**, 106 (2025), arXiv: 2412.14035
[3] M. Black, M. Lang, A. Lenz *et al*., JHEP **04**, 081 (2025), arXiv: 2412.13270
[4] M. L. Piscopo, A. Lenz, and A. V. Rusov, PoS **BEAUTY2023**, 028 (2024), arXiv: 2403.02267
[5] K. K. Shao, C. Huang, and Q. Qin, Eur. Phys. J. C **85**, 1011 (2025), arXiv: 2502.05901
[6] H. Y. Cheng, Chin. J. Phys. **78**, 324 (2022), arXiv: 2109.01216
[7] H. Y. Cheng and C. W. Liu, JHEP **07**, 114 (2023), arXiv: 2305.00665
[8] L. Dulibić, J. Gratrex, B. Melić *et al*., JHEP **07**, 061 (2023), arXiv: 2305.02243
[9] J. Gratrex, B. Melić, and I. Nišandžić, JHEP **07**, 058 (2022), arXiv: 2204.11935
[10] R. Aaij *et al*. (LHCb), Phys. Rev. Lett. **121**, 092003 (2018), arXiv: 1807.02024
[11] R. Aaij *et al*. (LHCb), Sci. Bull. **67**, 479 (2022), arXiv: 2109.01334
[12] K. K. Shao, H. L. Feng, X. Y. Liu *et al*., (2025), arXiv: 2509.11404
[13] R. Aaij *et al*. (LHCb), Phys. Rev. D **100**, 032001 (2019), arXiv: 1906.08350
[14] M. Ablikim *et al*. (BESIII Collaboration), Phys. Rev. D **107**, 052005 (2023)
[15] G. D'Agostini, arXiv: 1010.0632
[16] F. Bernlochner, A. Gilman, S. Malde *et al*., JHEP **05**, 061 (2025), arXiv: 2408.10063
[17] M. Fael, T. Mannel, and K. K. Vos, JHEP **12**, 067 (2019), arXiv: 1910.05234
[18] N. Gray, D. J. Broadhurst, W. Grafe *et al*., Z. Phys. C **48**, 673 (1990)
[19] D. J. Broadhurst, N. Gray, and K. Schilcher, Z. Phys. C **52**, 111 (1991)
[20] J. Fleischer, F. Jegerlehner, O. V. Tarasov *et al*., Nucl. Phys. B **539**, 671 (1999) [Erratum: Nucl. Phys. B **571**, 511 (2000)], arXiv: hep-ph/9803493
[21] K. Melnikov and T. v. Ritbergen, Phys. Lett. B **482**, 99 (2000), arXiv: hep-ph/9912391
[22] A. Boushmelev, T. Mannel, and K. K. Vos, JHEP **07**, 175 (2023), arXiv: 2301.05607
[23] A. H. Hoang, Z. Ligeti, and A. V. Manohar, Phys. Rev. Lett. **82**, 277 (1999), arXiv: hep-ph/9809423
[24] A. H. Hoang, Z. Ligeti, and A. V. Manohar, Phys. Rev. D **59**, 074017 (1999), arXiv: hep-ph/9811239
[25] A. H. Hoang and T. Teubner, Phys. Rev. D **60**, 114027 (1999), arXiv: hep-ph/9904468
[26] S. Aoki *et al*. (Flavour Lattice Averaging Group), Eur. Phys. J. C **80**, 113 (2020), arXiv: 1902.08191
[27] D. King, A. Lenz, M. L. Piscopo *et al*., JHEP **08**, 241 (2022), arXiv: 2109.13219
[28] F. Herren and M. Steinhauser, Comput. Phys. Commun. **224**, 333 (2018), arXiv: 1703.03751
[29] S. Navas *et al*. (Particle Data Group), Phys. Rev. D **110**, 030001 (2024)